Solar Phys (2007) 240: 37–48
DOI 10.1007/s11207-006-0247-6

Evolution of a Coronal Loop System

G. Tsiropoula · K. Tziotziou · T. Wiegelmann · Th. Zachariadis · C. Gontikakis · H. Dara

Received: 27 June 2006 / Accepted: 24 November 2006 / Published online: 1 March 2007

Abstract The temporal variation of a loop system that appears to be changing rapidly is examined. The analyzed data were obtained on 15 May 1999, with the Transition Region and Coronal Explorer (TRACE) during an observing campaign and consist of observations in the Fe IX/Fe X 171 Å and Fe XII 195 Å passbands taken at a cadence of ∼10 min. The special interest in this loop system is that it looks like one expanding loop; however, careful examination reveals that the loop consists of several strands and that new loop strands become visible successively at higher altitudes and lower loop strands fade out during the one hour of our observations. These strands have different widths, densities, and temperatures and are most probably consisting of, at least, a few unresolved thinner threads. Several geometric and physical parameters are derived for two of the strands and an effort is made to determine their 3D structure based on the extrapolation of the magnetic field lines. Electron density estimates allow us to derive radiative and conductive cooling times and to conclude that these loop strands are cooling by radiation.

Keywords Sun: transition region · Sun: loops · Sun: UV radiation

1. Introduction

High-resolution X-ray, XUV, and EUV observations from various spacecraft clearly indicate that active region plasmas are organized by the solar magnetic field into filamentary closed-loop structures. Furthermore, closed loops are recognized to be the fundamental constituent

G. Tsiropoula (✉) · K. Tziotziou
National Observatory of Athens, Institute for Space Applications and Remote Sensing, Lofos Koufos, GR-15236, Palea Penteli, Greece
e-mail: georgia@space.noa.gr

T. Wiegelmann
Max-Planck-Institut für Sonnensystemforschung, Max-Planck-Strasse 2, D-37191, Katlenburg-Lindau, Germany

Th. Zachariadis · C. Gontikakis · H. Dara
Academy of Athens, Research Center for Astronomy and Applied Mathematics, 4 Soranou Efesiou str., GR-11527, Athens, Greece

of the internal structure of the solar upper atmosphere. Thus, an essential first step toward the understanding of the solar corona and the construction of a realistic model of an active region is to determine observationally the behavior and physical properties of individual loops.

Most of the X-ray loops undergo little change in either structure or brightness throughout the greater part of their lifetime, but, some of them, especially EUV loops, show a dynamic behavior. For example, Levine and Withbroe (1977) described a loop that undergoes a "dramatic evacuation" of 70% of its mass, with hot material cooling and falling and cooler lines showing successively later maxima in brightness. They suggested that the cause of this behavior is the sudden cessation or substantial reduction of heating.

New observations with TRACE reported by Schrijver (2001) suggest that cooling and evacuation of non-flaring loops observed in the EUV lines is a rather common process. Relatively cool material seems to move downward at speeds of up to 100 km s^{-1}. Presumably, a drastic and fast reduction of the heating at the top of the loop should occur to produce high velocities. One consequence of this cooling process is that EUV emission peaks first in the hotter filter images and then in the cooler ones. Aschwanden *et al.* (2000) reported that the cooling of EUV loops in the $\sim$1 MK temperature range is dominated by radiative losses. Recently, Winebarger, Warren, and Seaton (2003) examined the temporal evolution of five cooling loops observed with TRACE. From the measured delays in appearance between the 195 and 171 Å filter images they estimated the cooling time of the loops and found that for four loops the measured lifetime is much longer than the expected lifetime of a cooling loop. They proposed that one way to reconcile this contradiction is to use the suggestions of Warren, Winebarger, and Mariska (2003), *i.e.*, that the loops are composed of multiple strands, which are each heated independently and sequentially.

The derivation of the properties of "individual" coronal loops is a fundamental problem, since current resolution limits the observed signal to always being a superposition of emission from several coronal structures found along the line of sight. In a recent work Aschwanden and Nightingale (2005) presented a quantitative analysis of the multistrand structure of coronal loops observed in the three TRACE filters. They also present observational signatures of multistrand loops (single, multiple, resolved, non-resolved, isothermal, and multithermal) and the corresponding cross-sectional flux profiles. They were able to resolve "elementary" or "monolithic" loop strands in terms of isothermal homogeneity, while Aschwanden (2005) provides three criteria that help to discriminate between elementary loop strands and composite loops. According to his results elementary loop strands (1) are nearly isothermal ($dT \lessapprox 0.2$ MK), (2) have a small width ($w \lessapprox 2$ Mm), and (3) have a faint contrast ($c \lessapprox 0.3$), whereas loop structures with larger widths and higher contrasts consist of heterogeneous composites.

In this work we study the evolution of a loop system observed with TRACE. The special interest in this loop system is that it is highly dynamic, changing rapidly with time. It looks like one loop increasing in height; however, careful examination reveals that the loop consists of several strands and that new strands become visible successively at higher altitudes and lower strands fade out during the one-hour coverage of our observations. Although, to our knowledge, no TRACE observations of loops showing the behavior of the loop system examined in this work have been presented so far, there have been several works in the past reporting loops that appear to increase in height by using Hα and X-ray observations (see, *e.g.*, Švestka *et al.*, 1987; Schmieder *et al.*, 1995; van Driel-Gesztelyi *et al.*, 1997; Kamio, Kurokawa, and Ishii, 2003). From the present observations we deduce values for some physical and geometrical parameters and estimate cooling times.

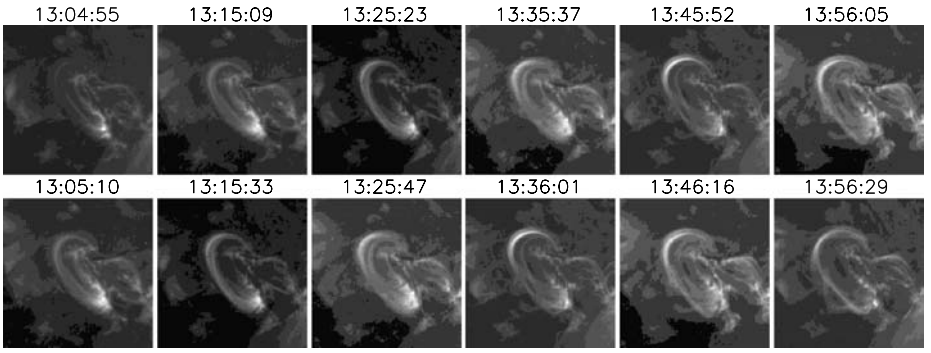

Figure 1 Time sequence images of the loop system ($100'' \times 100''$) observed with TRACE at 171 Å (first row) and 195 Å (second row) with a time cadence of ∼10 min.

2. Observations

The active region NOAA 8541 was observed on 15 May 1999. A sequence of TRACE images was obtained at 171 Å, 195 Å, 1600 Å, Lyα 1216 Å, and white light with a time cadence of ∼10 min. All data have a field of view of 1024 pixels × 1024 pixels and are at full resolution (1 pixel = 0.5″). The TRACE instrument is described in detail by Handy *et al.* (1999). The principal lines in the 171 channel are Fe IX/Fe X with a peak at 0.95 MK and in the 195 channel the Fe XII with a peak at 1.4 MK. The TRACE 171 and 195 Å passbands are sensitive in the combined temperature range ∼0.6 – 1.6 MK. All data have been corrected for a constant dark current, a CCD readout pedestal value of 87 Data Numbers (DN), hot pixels, and radiation spikes from cosmic rays and have been co-aligned by a cross-correlation technique to correct for solar rotation and spacecraft pointing jitter. To compensate for lack of uniform exposures each image is normalized in brightness by dividing by its own exposure time (*i.e.*, 19.48 s for the 195 Å images and 16.38 s for the 171 Å images). The active region consists of a large number of loops of various lengths that mostly seem to be constant in space and time. We focus on a region with a size of $100'' \times 100''$ containing a dipolar loop system that shows prominent variability (Figure 1). We study the temporal evolution of the loop observed at 171 and 195 Å in the time interval from 13:04:55 UT through 13:56:29 UT containing six images in each wavelength. Observations of the active region NOAA 8541 with a time cadence of 24 s were also available, but the field of view was equal to 768 pixels × 768 pixels, and, unfortunately, the region of interest was outside it. Images of the region obtained in the Lyα and C IV channels have also been examined, but there the loops could not be identified.

During TRACE observations high-cadence full-disk MDI magnetograms were also obtained. These magnetograms were used for the extrapolation of the magnetic field lines with the help of a linear force-free magnetic field model.

3. Results

3.1. Morphological Description and Evolution of the Loop System

For the study of the spatial and thermal evolution of the loop system in the 1-hour time coverage, two panels of six images are generated showing the intensity at 171 Å and at 195 Å (Figure 1, first and second row, respectively).

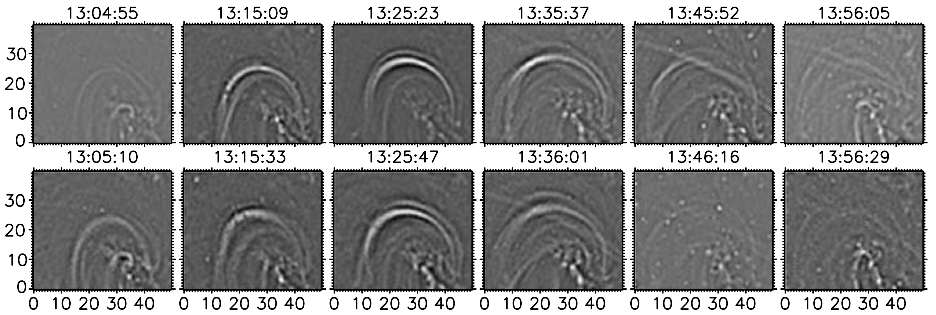

Figure 2 Laplacian of the brightness at 171 Å (first row) and 195 Å (second row) of the upper part of the loop system rotated by 30° in six consecutive frames taken ∼10 min apart.

Both bands show a series of individual (not clearly resolved) loops that connect the positive polarity magnetic flux concentrations in the southeast (lower part of the image) to the negative polarity concentration in the northwest (upper part of the image). These loops seem to be intersecting or overlapping in projection and evolving in intensity and height. New loops appear successively at a higher position, giving the impression of a loop system expanding upward. Toward the end of the time sequence more strands seem to split off at the upper part of the loop system, while later the loops become gradually weaker and the brightening declines steadily. The multiloop structure and its evolution is more evident in Figure 2, which shows the Laplacian of the brightness of the upper part of the 171 and 195 Å loops (after rotating by 30° the original images shown in Figure 1). The Laplacian acts as a high-pass filter, removing diffuse features and preserving structures with well-defined edges. From the Laplacian images it is obvious that what seems as expanding motion of the loops is not real but only apparent and that new loops appear successively above the lower ones. To show more clearly this variability we have averaged the fluxes over a stripe extending 2″ on either side of an axis passing vertically from the apexes of the loop system in all images (both original and Laplacian) of the time sequence and from the inner to the outer part of the loop system. In Figures 3 and 4 we plot the 171 Å (solid line) and the 195 Å (dotted line) flux distributions along these stripes beginning from the inner part (*i.e.*, from its footpoints side) of the loop system to the external part. In both figures one can see that as time progresses there is a clear displacement of the flux maxima toward larger x values.

From Figure 4 it is obvious that what seems as one loop increasing in height in Figure 3 is only apparent and that at least four loops can be distinguished in four discrete positions, *i.e.*, at ∼12″, 15″, 18″, and 21″ – 22″. It is also obvious that the displacement of the maxima in Figures 3 and 4 as time progresses occurs because new loops become visible successively at higher altitudes and lower loops fade out.

3.2. Determination of Physical Parameters

In the following we restrict our analysis only at the loop apex, since it seems rather complicated to separate the loop legs from the ambient background.

The cross-sectional flux profile passing from the loop top has no clear single peak and this result provides evidence for the existence of multiple, not clearly resolved, strands. We examine the evolution of the loop strand having a peak in the Laplacian of the flux observed at ∼18″. In the first frame of our observations the flux of the strand at 171 Å is lower than the flux at 195 Å. Subsequently, both fluxes increase till the third frame, but the increase of

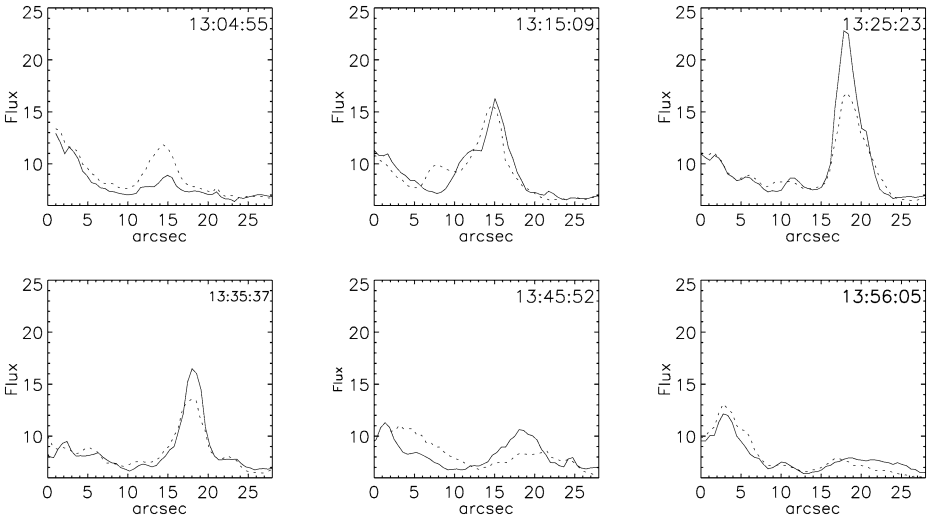

Figure 3 Changes of the fluxes (in DN s^{-1} px^{-1}) across the top of the loop at 171 Å (solid line) and 195 Å (dotted line) in six consecutive frames taken ∼10 min apart.

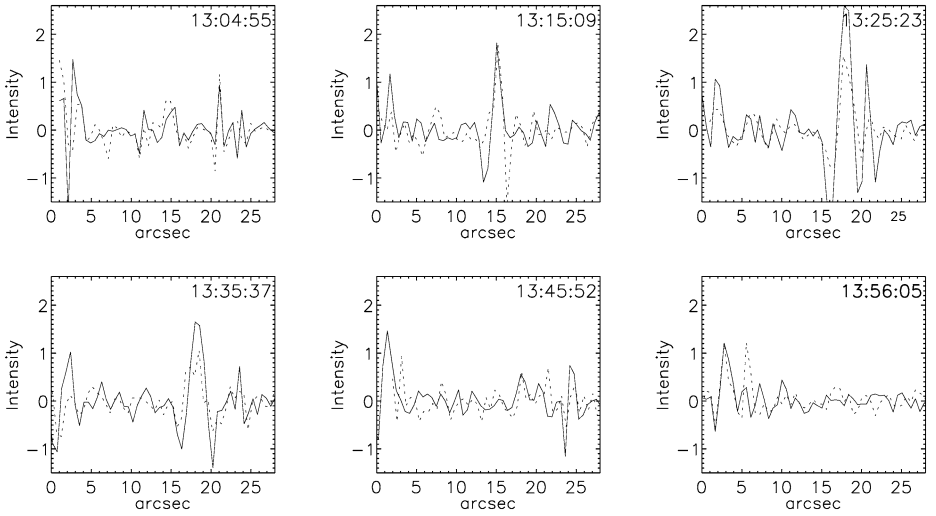

Figure 4 Changes of the Laplacian of the brightness across the top of the loop at 171 Å (solid line) and 195 Å (dotted line) in six consecutive frames taken ∼10 min apart.

the flux at 171 Å is significantly larger. Afterward both fluxes decrease until the end of the sequence (the flux at 171 Å remaining always larger than the corresponding flux at 195 Å), where they almost attain the value of the local background. The following explanation can be given to this behavior: Material hotter than the formation temperature of Fe XII cools, resulting in a decrease of the Fe XII emission. As it continues to cool below the formation temperature of this element the emission at the 171 Å channel increases. Then emission in both channels is decreasing, which means that the material continues cooling. Toward the

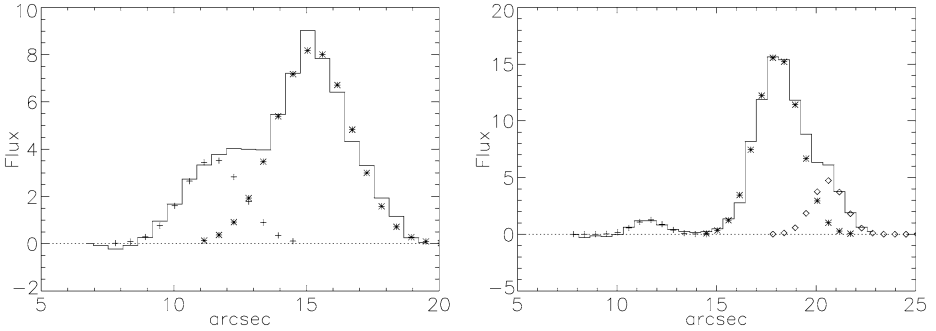

Figure 5 Changes of the background-subtracted fluxes (shown with histograms) and two or three Gaussian fits to the fluxes (with plus, asterisks, and diamonds) across the top of the loop system at 171 Å observed at 13:15:09 UT (left panel) and 13:25:23 (right panel).

end of the time sequence it is difficult to detect the loops against the background. The same behavior shows the loop strand observed at $\sim 15''$, which, however, is hardly detected after the second frame. Unfortunately, the low cadence of the data does not allow the calculation of detailed light curves, which should be more accurate to determine the evolution of the loops. There is, however, one more argument that supports our conclusion that the loops are cooling: The ratio of the fluxes (195 Å/171 Å) is larger than 1 at the beginning of the observations and then decreases to a value lower than 1 (Figure 3). Then one can conclude from the ratio of the response functions that the temperature of the threads is larger at the beginning and then decreases.

When the loop cools through a passband, the maximum of the flux $F(t)$ is detected at the time when the loop temperature matches the peak of the response function. Thus the peak flux F_{171} of the light curve in the cooler filter corresponds to the emission measure (EM) at the filter temperature $T_{171} = 0.95$ MK,

$$F_{171} = \mathrm{EM}\, R_{171} = \langle n_e^2 \rangle w R_{171}, \tag{1}$$

where F_{171} is in units of DN px^{-1} s^{-1}, $\langle n_e^2 \rangle$ is the mean square of the electron density, w is the width of the loop strand, and $R_{171} = 1.1 \times 10^{-26}$ DN px^{-1} s^{-1} cm^5 is the response function at $T = 0.95$ MK for the 171 Å filter when coronal abundances are assumed.

To isolate the emission originating only from the loop we must subtract the background emission, which at each wavelength and each time is taken as a linear function estimated from the fitting of several observed points taken on both sides of the loop boundaries. The changes of the background-subtracted fluxes can be parametrized with one, two, or more Gaussian functions, each one having three free parameters: peak value, peak position, and Gaussian width σ_w. This last parameter is related to the width of the loop w, taken as the FWHM of the Gaussian, by $w = 2\sigma_w(2\ln 2)^{1/2} = 2.35\sigma_w$. From the above relation an estimate for the electron density n_e can be obtained by assuming that the loop has a circular cross section. The background-subtracted peak fluxes and the geometrical thicknesses for the loop strands observed at $15''$ and at $18''$ are estimated from the fitting with two Gaussians of the flux variation curve across the top of the loop system at 13:15:09 UT (Figure 5, left) and with three Gaussians of the flux variation curve at 13:25:23 UT (Figure 5, right), respectively. The Gaussian parameters and the 1σ errors are found equal to: peak fluxes (8.27 ± 0.66) DN pixels^{-1} s^{-1} and (15.96 ± 0.72) DN pixels^{-1} s^{-1}, peak positions at $15.25'' \pm 0.20''$ and $18.06'' \pm 0.1''$, and widths (2.41 ± 0.48) Mm and (1.87 ± 0.17) Mm,

respectively. From these values and from Equation (1) electron density values equal to $(1.77 \pm 0.34) \times 10^9$ cm^{-3} and $(2.79 \pm 0.28) \times 10^9$ cm^{-3} are obtained for the tops of the loop strands observed at 15″ and 18″, respectively. If the loop strands are uniformly filled with plasma then n_e is the actual density. If, however, the loops consist of many unresolved thinner strands, the density given by $\langle n_e^2 \rangle^{1/2}$ is less than the actual density by the square root of the filling factor f, where f is the fraction of the volume of the loop filled by plasma. That the loops most likely consist of more strands comes out from Aschwanden's (2005) criterion regarding the contrast of the resolved strands. Thus, although their width is rather low, their contrast expressed as $(F - B)/B$ (where F is the observed flux and B the flux of the background) is greater than 0.3, as can easily be seen in Figure 3.

3.3. Determination of the 3D Structure of the Loop System

From TRACE observations we only have information on the 2D projection of the loop system. Knowledge of the 3D magnetic field structure can give information about the 3D structure of the observed TRACE loops, because the high conductivity of the coronal plasma enables the emitting plasma to outline the magnetic field lines. In the coronal part of the loops the magnetic pressure dominates the plasma pressure and the field is approximately force-free such that

$$(\nabla \times \mathbf{B}) = \alpha \mathbf{B}, \tag{2}$$

$$\mathbf{B} \cdot \nabla \alpha = 0, \tag{3}$$

where $\mathbf{B}$ is the magnetic field and α is the force-free parameter. The force-free parameter α is in general a function of space. Taking this into account corresponds to the non-linear force-free approach; see, *e.g.*, Wiegelmann (2004). A popular simplification is to choose $\alpha =$ constant in the entire computational domain, the linear force-free approach. The choice $\alpha = 0$ corresponds to potential fields. A comparison of observed and extrapolated magnetic fields in a newly developed active region by Wiegelmann *et al.* (2005a) revealed that a force-free model reconstructs the observed loop structures much better than a potential field. Linear force-free fields are in particular popular, because one needs only the line-of-sight photospheric magnetic field as input. We solve Equations (2) and (3) with the help of a Fourier transform method developed by Alissandrakis (1981). We use the photospheric line-of-sight magnetic field (measured with SOHO/MDI) as input. The force-free parameter α is unknown a priori. We compute the optimal value of α by comparing the reconstructed magnetic fields (with different values of α) with TRACE images. The method has been previously applied to data from SOHO/EIT in Marsch, Wiegelmann, and Xia (2004), to YOHKOH/SXT in Carcedo *et al.* (2003), and to EIT and Hα in Wiegelmann *et al.* (2005b). The latter work also contains details of an automated feature recognition technique based on coronal magnetic field models.

Within this work we apply the method to TRACE data. After all 3D field lines are projected onto the 2D TRACE image the deviation is measured between the projected magnetic field lines and the TRACE loop for different α values. The magnetic loop with the smallest deviation to the TRACE loop is the optimal field line for a given α value. The procedure is repeated with different values of α. As a result we obtain the optimal loops as a function of α and the minimum of these functions corresponds to the optimal force-free parameter α.

In Figure 6 we show the optimal linear force-free field line projected on the Laplacian of the TRACE image at 13:15 UT. The optimal value for α is found to be equal to 10^{-7} m^{-1}.

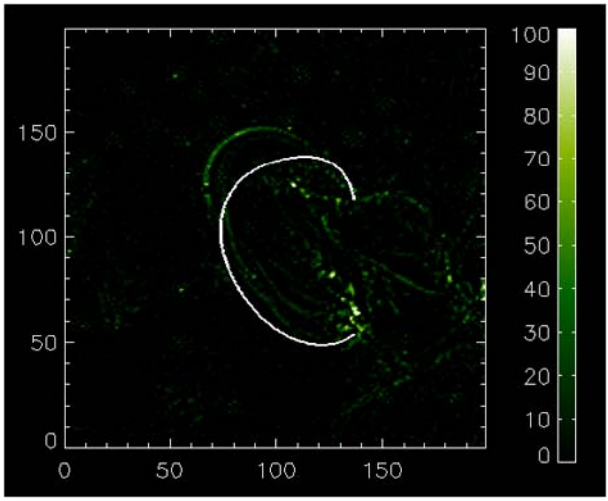

Figure 6 Projection of the main center loop computed with a linear force-free magnetic field model by using the optimal force-free parameter $\alpha = 10^{-7}$ m^{-1} on the Laplacian of the 171 Å TRACE image observed at 13:15:09 UT. The deviation between the linear force-free magnetic field line and the loop is probably due to the limitations of using a linear force-free model for the extrapolation of the magnetic field line.

The magnetic loop has a length of 72.5 Mm, a maximum loop height of 11.7 Mm, an azimuth of 90°, and an inclination of 68°. The deviation between the magnetic field line and the TRACE loop is most probably the result of the approach used of the force-free field. More sophisticated models, e.g., non-linear force-free fields, could give magnetic field lines that would agree with the TRACE loops even better than the best linear force-free field line. Because the magnetic loops and the TRACE loops show some deviation we calculate the total length of the TRACE loops by simulating the observed loops with magnetic lines having the same height profile and get corrected loop lengths of 85.0 Mm for the loop strand observed at 15″ and of 92 Mm for the loop strand observed at 18″.

3.4. Cooling Times

In a general case and in the absence of energy input, the cooling of the loop plasma is due to radiation or conduction or both. In the initial phase of the loop evolution, conductive cooling dominates, but at some point there is a transition to radiative cooling (Antiochos and Sturrock, 1982). Radiative and conductive processes are associated with the radiative and conductive cooling times given, respectively, by

$$\tau_{\rm rad} = \frac{E_{\rm th}}{{\rm d}E_R/{\rm d}t} = \frac{3k_{\rm B}T}{n_{\rm e}\Lambda(T)} \approx \frac{2.12\times10^3 T^{3/2}}{n_{\rm e}} \tag{4}$$

and

$$\tau_{\rm cond} = \frac{3n_{\rm e}k_{\rm B}L^2}{\kappa} \approx 3.7\times10^{-10}\, n_{\rm e}T^{-5/2}L^2. \tag{5}$$

In these equations, as is shown by Martens, Kangelborg, and Berger (2000), a good approximation to the radiative loss curve in the TRACE-sensitive temperature range is given by

$$\Lambda(T) \approx 1.95\times10^{-19}T^{-1/2}, \tag{6}$$

in erg cm^3 s^{-1}, and $\kappa = \kappa_0 T^{5/2} = 1.1\times10^{-6}\,T^{5/2}$ erg s^{-1} cm^{-1} K^{-1} is the Spitzer thermal conductivity, $k_{\rm B}$ is Boltzmann's constant, and L is the loop half-length. Comparison of these

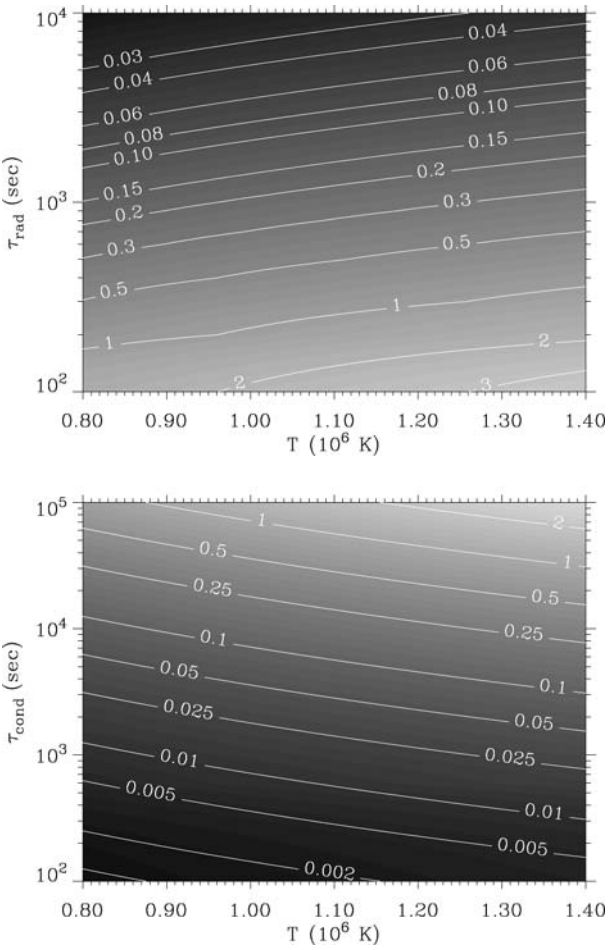

Figure 7 Changes of τ_{rad} and τ_{cond} as a function of temperature for a loop half-length equal to 44.0 Mm. Contours of electron density inside the figure are in units of 10^{10} cm^{-3}.

two cooling times as a function of temperature for a loop half-length equal to 44.0 Mm (mean half-length of the observed strands) is given in Figure 7. Contours of electron density are given on the figure. The temperatures and densities for these expressions are to be evaluated at the beginning of the cooling process. Moreover, it is important to realize that temperature and electron density are average quantities in the coronal part of the loop and that τ_{cond} and τ_{rad} do not account for the evolution of these two quantities as the loop cools. Hence they cannot be used to estimate the time a loop takes to cool from one temperature to another. To estimate the cooling times of the two loop strands we take as initial temperature value the peak temperature at the 195 Å filter, *i.e.*, $T = 1.4 \times 10^6$ K, electron densities of 1.77×10^9 and 2.79×10^9 cm^{-3}, and loop half-lengths of 42.5 and 47.0 Mm, respectively. We assume that electron densities are constant during the cooling, since as is shown in numerical simulations (see, *e.g.*, Serio *et al.*, 1991) the density decays at half the rate of temperature. We find radiative cooling times equal to 2000 and 1270 s and conductive cooling times equal to 5087 and 9785 s, respectively, implying that both loops are cooling by radiation. The derived radiative cooling times are longer than the cadence and are consistent with the observations, since we see the features in more than one image.

As can be seen from Figure 7 for the same range of temperatures conduction dominates at low densities and radiation dominates at the high ones. Thus there is a value of the electron density for which there is a passage from one state to the other. We can find this value from the following: When the plasma is cooling both radiatively and conductively, then the total cooling time is

$$\frac{1}{\tau_{\rm tot}} = \frac{1}{\tau_{\rm rad}} + \frac{1}{\tau_{\rm cond}}, \tag{7}$$

which gives

$$\tau_{\rm tot} = \frac{n_{\rm e} L^2 T^{3/2}}{4.71 \times 10^{-4} L^2 n_{\rm e}^2 + 2.7 \times 10^9 T^4}. \tag{8}$$

Clearly the total cooling time depends on the loop's half length, density, and temperature. In Figure 8 the total cooling time as a function of electron density is shown for different temperature and half-length values. For the considered temperature range it can be seen that as the electron density decreases the total cooling time increases for increasing loop length. For a loop with given temperature and length and in the absence of energy input a reasonable bound of the density $n_{\rm e}^b$ in the loop plasma for which there is a passage from the conduction dominating state to the radiative one can be obtained by equating the radiative and conductive loss rates. This electron density is obtained by setting the derivative of Equation (8) with respect to density equal to zero, which gives

$$n_{\rm e}^b = 2.39 \times 10^6 \frac{T^2}{L}. \tag{9}$$

For the loops we are considering, by taking an initial temperature in the range $(1.4-1.6) \times 10^6$ K and half-lengths of 42.5 and 47 Mm a reasonable value of the density in the loop plasma for which there is a passage from the conduction dominating state to the radiative one is $\sim 1.0 \times 10^9$ cm^{-3}. This value is lower than the values estimated from Equation (1) and strengthens the conclusion that these loops are cooling by radiation. From Figure 8 one can also conclude that loops with longer lengths have larger total cooling times. Although we have not performed detailed calculations, the apparent constancy in time of the larger loops observed in AR8541 is most likely due to their larger total cooling times.

The actual cooling times may be shorter than these given estimates, since, *e.g.*, the density is assumed to be constant during the cooling process and the effect of the filling factor was not taken into account. It is obvious that smaller filling factors give shorter radiative cooling times and longer conductive cooling times.

4. Summary and Conclusions

We analyzed a loop system observed with TRACE simultaneously in the 171 and 195 Å passbands. This loop system was highly dynamic and gave the impression as increasing in height and expanding laterally during the one-hour coverage of our observations. Our analysis, however, revealed that the loop consisted of several loop strands and that while lower strands fade out higher strands became visible. We were able to resolve and to localize several loop strands by taking the Laplacian of the original images, which acts as a high-pass filter. We estimated emission measures, electron densities, and widths at the tops of two of the resolved loop strands and tried to reconstruct their 3D structure by extrapolating

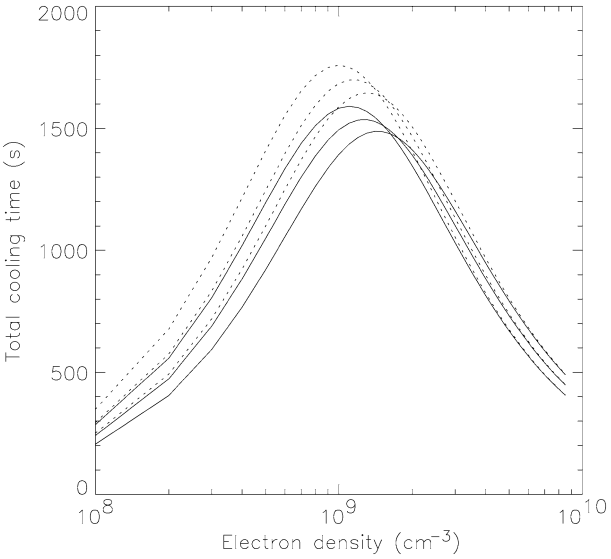

Figure 8 The total cooling time (in seconds) as a function of electron density for different values of temperature and loop half-lengths. Full lines correspond to $L = 42.5$ Mm and dotted lines to $L = 47$ Mm. In each set of curves the outer (from the left) corresponds to $T = 1.4$ MK, the one at the middle to 1.5 MK, and the inner one to 1.6 MK.

the magnetic field lines using MDI observations. We calculated radiative and conductive cooling times and concluded that the examined loop strands are cooling by radiation.

Our analysis suggests the need for high spatial resolution observations when attempting to analyze the properties of coronal loops. With the TRACE 1″ resolution we were able to show that the observed loop system consisted of several loop strands, each one having different electron densities and widths (and temperatures) and different thermal evolution. However, according to Aschwanden's (2005) criteria these loop strands most likely consisted of finer unresolved threads. This implies that the obtained physical parameters still represent statistical averages sampled over a finite number of elementary substructures

Acknowledgements The authors would like to thank the TRACE team for providing data and the anonymous referee for useful comments and suggestions that helped to improve the paper. K. Tziotziou acknowledges support by Marie Curie European Reintegration Grant No. MERG-CT-2004-021626. The work of T. Wiegelmann is supported by DLR Grant No. 50 OC 0501. G. Tsiropoula is grateful to M. Aschwanden and S. Antiochos for useful suggestions.

References

Alissandrakis, C.E.: 1981, *Astron. Astrophys.* **100**, 197.
Antiochos, S.K., Sturrock, P.A.: 1982, *Astrophys. J.* **254**, 343.
Aschwanden, M.J.: 2005, *Astrophys. J.* **634**, L193.
Aschwanden, M.J., Nightingale, R.W.: 2005, *Astrophys. J.* **633**, 499.
Aschwanden, M.J., Tarbell, T.D., Nightingale, R.W., Schrijver, C.J., Title, A., Kankelborg, C.C., *et al.*: 2000, *Astrophys. J.* **535**, 1047.
Carcedo, L., Brown, D.S., Hood, A.W., Neukirch, T., Wiegelmann, T.: 2003, *Solar Phys.* **218**, 29.
Handy, B.N., Acton, L.W., Kankelborg, C.C., Wolfson, C.J., Akin, D.J., Bruner, M.E., *et al.*: 1999, *Solar Phys.* **187**, 229.
Kamio, S., Kurokawa, H., Ishii, T.: 2003, *Solar Phys.* **215**, 127.
Levine, R.H., Withbroe, G.L.: 1977, *Solar Phys.* **51**, 83.
Marsch, E., Wiegelmann, T., Xia, L.D.: 2004, *Astron. Astrophys.* **428**, 629.
Martens, P.C.H., Kangelborg, C.C., Berger, T.E.: 2000, *Astrophys. J.* **537**, 471.
Schmieder, B., Heinzel, P., Wiik, J.E., Lemen, J., Anwar, B., Kotrč, P., Hiei, E.: 1995, *Solar Phys.* **156**, 337.

Schrijver, C.J.: 2001, *Solar Phys.* **198**, 325.
Serio, S., Reale, F., Jakimiec, J., Sylwester, B., Sylwester, J.: 1991, *Astron. Astrophys.* **241**, 197.
Švestka, Z., Fontenla, J., Machado, M., Martin, S., Neidig, D.: 1987, *Solar Phys.* **108**, 237.
van Driel-Gesztelyi, L., Wiik, J.E., Schmieder, B., Kitai, R., Tarbell, T., Anwar, B., Funakoshi, Y.: 1997, *Solar Phys.* **174**, 151.
Warren, H.P., Winebarger, A.R., Mariska, J.T.: 2003, *Astrophys. J.* **593**, 1174.
Wiegelmann, T.: 2004, *Solar Phys.* **219**, 87.
Wiegelmann, T., Lagg, A., Solanki, S.K., Inhester, B., Woch, J.: 2005a, *Astron. Astrophys.* **433**, 701.
Wiegelmann, T., Inhester, B., Lagg, A., Solanki, S.K.: 2005b, *Solar Phys.* **228**, 67.
Winebarger, A.R., Warren, H.P., Seaton, D.B.: 2003, *Astrophys. J.* **593**, 1164.